Fluidic Optics

George M. Whitesides* and Sindy K.Y. Tang
Department of Chemistry and Chemical Biology, Harvard University
12 Oxford St., Cambridge, MA 02138

ABSTRACT

Fluidic optics is a new class of optical system with real-time tunability and reconfigurability enabled by the introduction of fluidic components into the optical path. We describe the design, fabrication, operation of a number of fluidic optical systems, and focus on three devices – liquid-core/liquid-cladding (L^2) waveguides, microfluidic dye lasers, and diffraction gratings based on flowing, crystalline lattices of bubbles – to demonstrate the integration of microfluidics and optics. We fabricate these devices in poly(dimethylsiloxane) (PDMS) with soft-lithographic techniques. They are simple to construct, and readily integrable with microanalytical or lab-on-a-chip systems.

Keywords: poly(dimethylsiloxane); soft lithography; microfluidics, waveguides; dye lasers; bubbles; fabrication

1. INTRODUCTION

"Fluidic optics" (also, interchangeably, called "optofluidics") is the study of a class of optical system that involves at least one fluidic component in the functional optical path. The incorporation of fluids into optical systems offers a simple and cost-effective method of fabricating high-quality optical structures, and enables real-time tunability of optical properties that are difficult to reconfigure in conventional solid-state optical systems. The introduction of fluids in the optical path also facilitates the integration of on-chip light sources and sensors with microfluidic analytical systems for biomedical and biological analyses.

The fluidic components in optofluidic systems can be either static or dynamic. Examples of static fluidic optical components include tunable liquid lenses, mercury mirrors in liquid mirror telescopes[1], and droplet resonators.[2] Due to minimization of surface energy, the fluid/fluid interface is intrinsically smooth. For dynamic systems in microfluidic channels (typical length scale < 500 μm), the flow takes place in the regime where the Reynolds number is low (Re ~ 5–500).[3] In this regime, laminar flow dominates, and the interface between different liquid streams in these systems is optically smooth.

An additional characteristic of dynamic fluidic systems is ease with which the liquids can be replaced and/or replenished continuously. This capability for replenishment allows injection of liquids with different properties (e.g., index of refraction, absorption, fluorescence) to tune the optical output of the system in real time. Furthermore, by manipulating the flow conditions, it is possible to adjust the path and geometry of light beam inside these fluidic devices continuously. Finally, this replacement makes photobleaching and related phenomena relatively unimportant, since the component that is bleached is replaced continuously. These advantages are, of course, purchased at the price of increased complexity: these systems are more complicated to operate (although simpler to fabricate) than solid-state optical systems.

Optofluidics, edited by Demetri Psaltis, Yeshaiahu Fainman, Proc. of SPIE Vol. 6329, 63290A, (2006) · 0277-786X/06/$15 · doi: 10.1117/12.681672

In this paper, we limit our discussions to dynamic fluidic optical systems: that is, systems in which the optical properties of the systems *require* that the liquids in the optical path are flowing. We: i) describe the fabrication of fluidic optical devices using soft lithography, and ii) give examples of fluidic optical devices – liquid-core/liquid-cladding (L^2) waveguides,[4-7] on-chip light sources[8-10], and bubble diffraction grating[11] – to demonstrate the design and operation of fluidic optical systems.

2. FABRICATION AND MANIPULATION OF LIQUIDS IN MICROFLUIDIC SYSTEMS

We fabricate fluidic optical systems in poly(dimethylsiloxane) (PDMS) using the techniques in soft lithography.[12-24] PDMS is one of the most actively developed polymers for microfluidics. Fabrication in PDMS is easy, and its use as a material reduces the time, complexity, and cost of prototyping; its influence on costs of manufactured systems remains to be established, but polymers are, in general, less expensive than ceramics as materials. PDMS has a refractive index of ~ 1.4. It is transparent in the visible range (240 nm – 1100 nm) with an extinction coefficient of $< 10^{-10}$,[25] and has negligible birefringence.[26] It is therefore possible to enclose fluidic optical components in PDMS, and couple light through PDMS, with minimal loss due to absorption. Commercially available PDMS—Silgard 184—does, unfortunately, contain nanoparticles of silica that introduce unwanted scattering of light. In the devices we and others have fabricated, the thickness of PDMS for enclosure of microfluidic components is limited (usually < 1 cm), and thus scattering due to passage of light through PDMS does not cause significant loss during the coupling of light into and out of the devices.

The details of fabrication using soft lithography can be found elsewhere.[15,19-23] Here we provide a summary of the processes involved. The optical/microfluidic channels are designed in a CAD program and printed onto a high-resolution transparency (~5000 dpi). This transparency is used as a photomask in 1:1 contact photolithography to produce a master: this master consists of a positive bas-relief of photoresist on a silicon wafer, and serves as a mold for PDMS. Liquid PDMS pre-polymer is poured over the master and cured for 1 h at 70 °C. The PDMS replica is then peeled from the master and sealed to a flat PDMS, glass, or silicon surface to form the microfluidic channels. The overall process takes ~ 24 h. Figure 1 outlines the processes involved.

To introduce and recover fluids from microchannels, we use polyethylene tubing to connect holes bored in PDMS; we normally uses syringes to provide pressure or vacuum, and thus to drive the motion of fluid in the channels. We fabricate the holes bored into the PDMS to be slightly smaller than the outer diameter of the tubing; when the tubing is inserted, it exerts pressure on the PDMS and provides a waterproof seal. The polyethylene tubing also conforms to syringe needles. This ability allows for syringes (and syringe pumps) to be coupled easily to microfluidic channels.

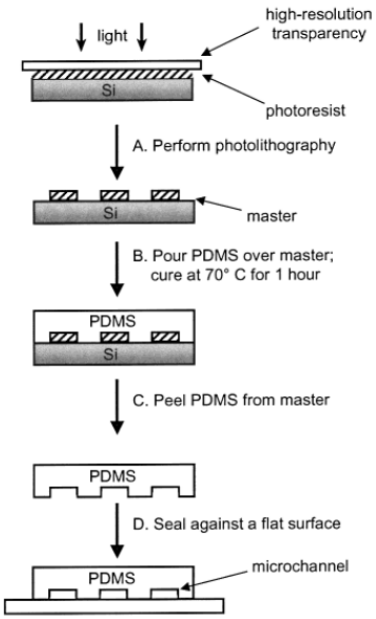

Fig.1. Scheme describing rapid prototyping of microfluidic systems. A system of channels is designed in a CAD program. A commercial printer uses the CAD file to produce a high-resolution transparency (~ 5000 dpi). (A) This transparency is used as a photomask in contact photolithography to produce a master. A master consists of a positive relief of photoresist on a silicon wafer and serves as a mold for PDMS. (B) Liquid PDMS pre-polymer is poured over the master and cured for 1 h at 70 °C. (C) The PDMS replica is peeled from the master, and (D) the replica is sealed to a flat surface to enclose the channels. The overall process takes ~ 24 h.

3. OPERATION OF FLUIDIC OPTICAL DEVICES

This section describes three devices to demonstrate the design, operation and characterization of fluidic optical systems.

3.1 Liquid-core/liquid-cladding (L^2) waveguides

3.1.1 *Construction of L^2 waveguides*. L^2 waveguides consist of two streams of liquids with lower refractive index (the cladding), sandwiching a stream of liquid with higher refractive index (the core) flowing in a microchannel.[4] The microchannels are fabricated in PDMS as described in the previous section. Light from an optical fiber is end-coupled into the guiding liquid. The output of the L^2 waveguide, where the core stream is forced to turn abruptly by 90°, can be imaged through an optically transparent window by using a microscope objective and a charge-coupled device, or through an additional inlet for an optical fiber at the end of the channel coupled to a photodetector. Figure 2A-C sketches a typical L^2 waveguide schematically.

In principle, any liquid that does not swell PDMS[27] can be used in L^2 waveguides, as long as the contrast in index of refraction between the core and the cladding streams are large enough to sustain the propagation of light. The contrast in the index of refraction can be provided by: (i)

liquids with different chemical composition,[4] e.g. aqueous solution of $CaCl_2$ (n_d = 1.445) as the core and deionized water (n_d = 1.335) as the cladding (figure 2A-D), (ii) a single homogeneous liquid (e.g. water) with a difference in temperature between the core and cladding ($\Delta T = T_{cladding} - T_{core} >$ 37 °C, corresponds to $\Delta n > 0.005$) perpendicular to the longitudinal axis of the waveguide (figure 2E),[7] or (iii) a suspension dielectric nanoparticles with different volume fractions, e.g. a suspension of polystyrene particles in water (diameter = 160 nm, volume fraction = 0.25 %) as the core, and pure water as the cladding (figure 2F).[5]

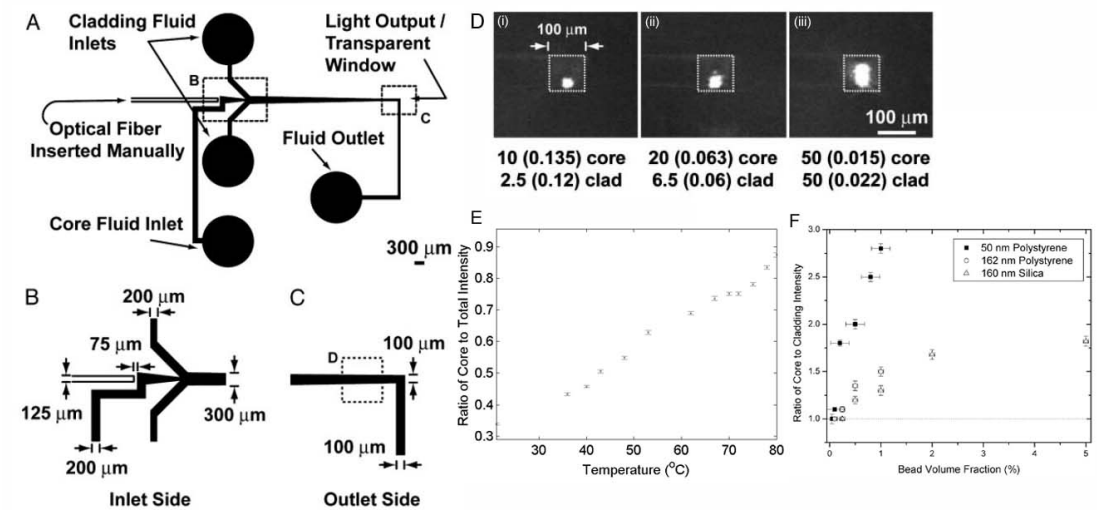

Fig.2. L^2 waveguide systems. (A) Diagram of the design of a microfluidic channel used in these experiments. (B–C) Detailed diagrams of the regions of the microfluidic channel in A highlighted by dashed boxes. (D) (i)-(iii) Optical micrographs of the cross section of the outlet of the microfluidic channel viewed through the transparent window. The dashed box shows the location of the cross section of the microfluidic channel. The rates of flow (μL/min) (and the residence time in seconds) of the core and the cladding (clad) are listed. The guided light was from a fiber-coupled laser with λ = 780 nm. (E) Plot of intensity ratio of core to total intensity as a function of temperature in the cladding region (total rate of flow = 60 mL/h , T_{core} = 21 °C). (F) Ratio of core to cladding intensity in the L^2 waveguide as function of volume fraction of nanoparticles.

3.1.2 *Characterization of L^2 waveguides.* We demonstrated both single- and multi-mode guiding by controlling the relative rates of flow of the core and cladding streams. Decreasing the ratio of flow rates of the core to the cladding streams decreases the core size from > 100 μm to < 10 μm, and thus switches the guiding from multi- to single-mode (figure 2D). At a rate of flow of 10 μL/min, the operating length of our L^2 waveguides is ~ 5 mm. This length is limited by diffusive broadening of the interface between streams, which decreases the contrast in refractive index between the core and the cladding. This unfavorable effect can be partially circumvented, however, by using a higher rate of flow. The efficiency of coupling light into a multimode optical fiber (step-index fiber, numerical aperture = 0.22, d_{core} = 105 μm, $d_{cladding}$ = 125 μm) from the L^2 waveguide was ~ 40%. Light exiting the L^2 waveguide remains polarized in the input direction to ~ 100:1; this ratio is indistinguishable from the light in the input fiber.

The loss in L^2 waveguides composed of liquids with different chemical composition is estimated to be < 1 dB/cm.

3.1.3 *Complex devices derived from L^2 waveguides.* Based on the L^2 waveguide configuration, we have developed other functional optical devices in microfluidic systems. (i) *Optical switch.*[4] A L^2 waveguide is branched into three separate channels. The relative rates of flow of the cladding liquids determine the path of the core liquid in this kind of microfluidic device, and thus the path of the light (figure 3A). (ii) *Evanescent coupler.*[4] This device consists of two L^2 waveguides sharing an inner cladding stream. Light from an optical fiber is introduced into one of the L^2 waveguides. The rate of flow of the liquids adjusts the width of the inner cladding stream, and thus the efficiency of coupling of evanescent fields between the two cores of the L^2 waveguides (figure 3B). (iii) *Diffusion-controlled splitter.*[6] In this device, light propagates in a direction opposite to that of the flow of liquids in two parallel L^2 waveguides; in the fluidic streams, diffusion cases the two guiding channels to merge smoothly into a single L^2 waveguide: that is, the light moves in the direction of decreasing extent of diffusive mixing. We demonstrated the ability of this system to split a single input beam into two output beams with equal intensities (figure 3C). .

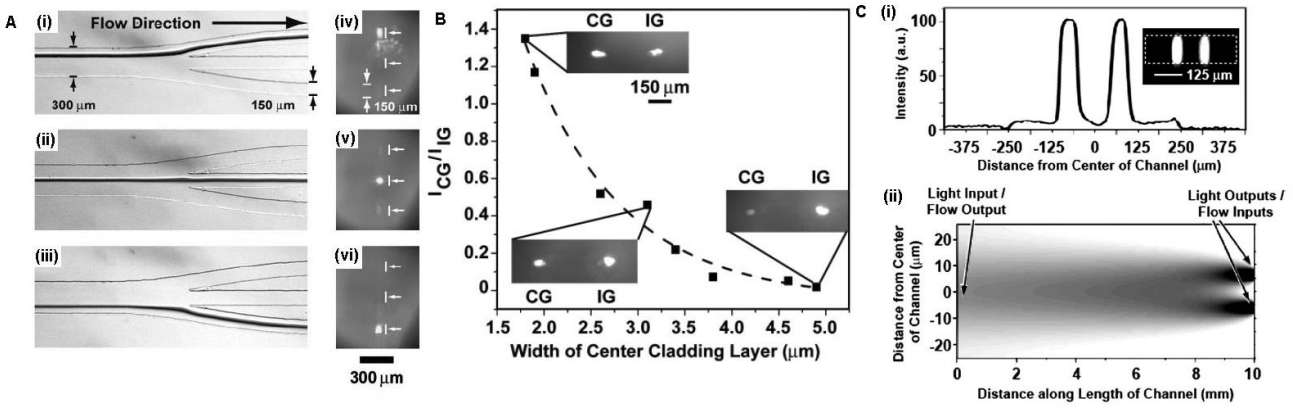

Fig.3. (A) *Optical switch.* (i)-(iii) Optical micrograph of the top view of the microfluidic channels. Dye in the core fluid makes it easily imaged; the dye is omitted in use. (iv)-(vi) Optical micrograph of the light that exits the L^2 waveguides at the end of the channel system. The white arrows and lines represent the location of the ends of the branches of the microfluidic channel. (B) *Evanescent coupler.* Plot of the ratio of the intensity of the light emitted from the coupled guide (ICG) and the illuminated guide (IIG). (Insets) Shown are optical micrographs of the cross section of the output of the microfluidic channels viewed through the transparent window. (C) (i) Plot of the profile of the intensity of light output as a function of distance from the center of the channel. The light (λ = 780 nm) was coupled into the L^2 waveguide from a single-mode optical fiber. The rate of flow of the core fluids was 2.5 μL/min, of the central cladding fluids was 5 μL/min, and of the outer cladding fluids was 10 μL/min. (Inset) Optical micrograph of light exiting the microfluidic channel, viewed through the transparent window. The dashed box shows the walls of the channel. (ii) Contour plot of the refractive index as a function of the distance from the center of the width of the channel and of the distance along the length of the channel. The gradient of gray scale from black to white indicates values of the refractive index from 1.431 to 1.414. Only the main portion of the waveguide (1 cm x 0.005 cm, l x w) is simulated.

Advantages and disadvantages of L^2 waveguides. To conclude our discussion of these systems, L^2 waveguides have two main advantages. (i) They are dynamic – their structure and function depend on a continuous, laminar flow of the core and cladding liquids, and can be reconfigured and adapted continuously in ways that are not possible with solid-state waveguides. By changing the liquid composition and the relative rates of flow between the core and cladding streams, we can switch between single- and multi-mode waveguiding, adjust the optical path, and tune the coupling efficiency between waveguides. (ii) They are easy to fabricate. Since the dimensions of the waveguiding region (i.e., the liquid core) in the flowing liquid streams are smaller than the dimensions of the channel, and because the roughness of the edges of the channel does not scatter light or otherwise degrade performance, L^2 waveguides can be fabricated easily and rapidly in organic polymers by using the convenient techniques of rapid prototyping (figure 4).

The L^2 systems also have prominent disadvantages, mainly: (i) a constant supply of fluids is necessary for both the cladding and the guiding streams (a supply of 250 mL is necessary to run one stream at 175 μL/min for 24 h). (ii) L^2 systems using water and PDMS are unable to guide light of the wavelengths (λ = 1,300–1,600 nm) used in telecommunications applications because of large absorptive losses in both the fluid streams and in the PDMS. (ii) The speed of optical switching is ~ 0.1 Hz. This value is much slower than switching in conventional planar waveguides (~ 1–100 GHz). Nevertheless, the system should meet the demands of applications that do not require fast switching, such as optical sensing and bioassays.

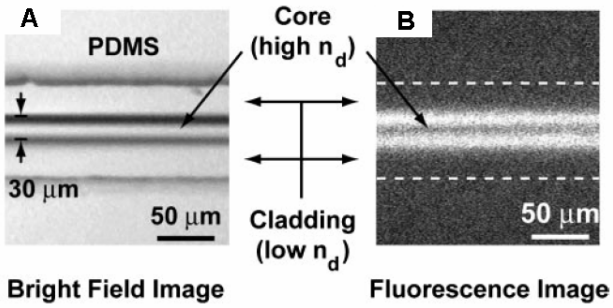

Fig.4. Optical micrograph of the L^2 waveguide in the region in the dashed box in C. The core fluid has been dyed to aid visualization. (B) Fluorescence micrograph of the same region of the channel as in A. The visible fluorescence signal has been produced by excitation with a broadband deuterium, fiber-coupled light source leaking into the evanescent field from the core of the waveguide. The dotted lines indicate the location of the walls of the microchannel.

3.2 Microfluidic light sources

We developed various on-chip fluidic light sources based on the L^2 waveguide systems for optical detection and spectroscopic analysis in integrated microanalytical systems (μTAS).[8-10] In these systems, the liquid cores contain fluorescent dyes, excited by incident light from an external halogen bulb or pump laser. Integration of fluorescent light sources during device fabrication removes both the need for insertion and alignment of conventional, optical-fiber light sources and

the constraints on channel size imposed by fiber optics, albeit at the cost of establishing a microfluidic infrastructure.

3.2.1 Microfluidic Dye Lasers

The construction of a microfluidic dye laser is similar to that of an L^2 waveguide.[9] Solutions of fluorescent dye act as the gain media. They form the core streams, sandwiched by cladding streams with lower index of refraction, in a microchannel of length 5 – 20 mm where the dye is pumped optically by an external laser source. The microchannel terminates at both ends with T-junctions coated with thin layers of gold or silver to act as mirrors for the optical cavity (figure 5).

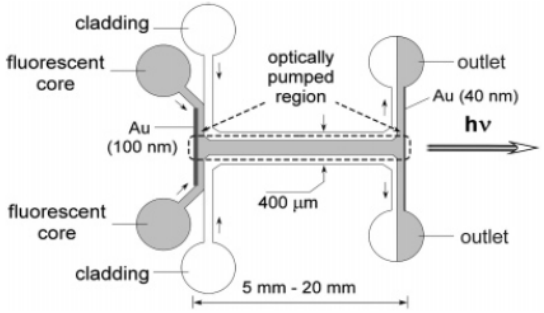

Fig.5. Top-view scheme for an L^2 waveguide laser consisting of a liquid cladding and fluorescent liquid core flowing laminarly in a microfluidic channel in PDMS (n_D = 1.41). The dimensions of the central channel were 100 μm x 400 μm x 10 μm (height x width x length). The 532-nm laser beam (frequency-doubled Nd:YAG, 50 Hz repetition rate, 16-ns pulse) was elongated with a cylindrical lens, and the optical pumping region covered the full length of the waveguiding region for a 10-mm-long channel.

We demonstrated lasing with 2-mM rhodamine 640 perchlorate in methanol as the core stream, and pure methanol as the cladding stream. A 532-nm pump laser beam (frequency doubled Nd:YAG, 50 Hz repetition rate, 16-ns pulse) is elongated and focused onto the microchannel with a cylindrical lens. At the rate of flow chosen in our experiments (32 –4 mL/h), the incoming pump pulse (50 Hz repetition rate) excited a given volume of the dye solution within the fluorescent core between 2 and 20 times. A high rate of flow ensures a rapid replenishment of the dye. Coupled with the short (16 ns) pulse length, we eliminated potential photobleaching of the dyes at the power levels used (up to 0.15 mJ/pulse).

Figure 6 is a plot of output power and line width as a function of pump power. At low pump power (<5 μJ/ pulse), the line width (full width at half-maximum, fwhm) of the emission is ~ 45 nm, with λ_{max} centered at 625 nm. The fwhm drops to ~4 nm between pump powers of 7 and 16 μJ. The threshold for lasing occurs at 22 μJ pulse energy. In systems with high $\Delta n = n_{core} - n_{cladding}$, where the light is strongly confined to the waveguide, we observed higher efficiencies of conversion and wider divergence angles (e.g., 24% and 100 mrad, respectively, for EG-core and methanol-cladding) than the systems with low Δn (e.g., 10% and 40 mrad, respectively, for methanol-core and methanol-cladding), where light is weakly confined to the waveguide.

We can tune the output wavelength of the laser by changing the choice and volume fraction of the solvent for the dye. Changing the solvent in the fluorescent core provides a simple means of adjusting the wavelength of emission for a given dye without incorporating dispersive elements

(prisms or gratings) into the optical cavity. For example, the wavelength of the light output for rhodamine 640 shifted by more than 20 nm by changing the composition of the core liquid; ìmax) 617 nm for methanol, 631 nm for EG, and 634 nm for DMSO. Furthermore, it is possible to tune λ_{max} continuously by adjusting the composition of a mixture of DMSO and MeOH in the core.

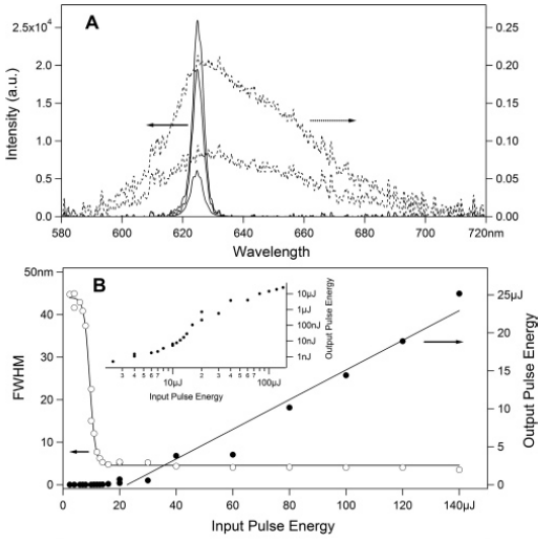

Fig.6. Output of the L^2 waveguide of Figure 5 containing 2 mM rhodamine 640 perchlorate in methanol as the core, and pure methanol as the cladding. (A) Emission spectra from L^2 fluorescent light source at different pump powers measured on-axis (note the x105 difference in scale for spectra at input powers below (dashed) and above (solid) threshold). (B) Dependence of the intensity of the optical output and line width (fwhm) on the energy of the pump pulse. The curves are drawn to guide the eye. Inset: output vs. input power on a log-log scale from data on integrated peak area.

3.3 Bubble diffraction grating

The use of immiscible fluids – emulsions, dispersions and foams – provides an additional route to periodic, self-assembled, geometries. Here we describe a tunable, fluidic, two-dimensional diffraction grating based on a microfluidic system comprising a flow-focusing (FF) bubble generator[28-39] and a flowing, regular lattice of bubbles formed by dynamic self-assembly.[11] The structure of these lattices can be tuned with switching times of less than ten seconds by changing the pressures and rates of flow applied to the device. These diffraction gratings exhibit high stability (over hours of operation if properly designed and operated).

The FF region comprises two inlet channels for the liquid phase, and a single inlet channel for the gaseous phase. The gas and liquid phases meet at a junction upstream of a narrow orifice. The gaseous thread periodically enters the orifice, breaks, and releases a bubble into the outlet channel; the frequency of bubble formation can be greater than 10 kHz. We can control the volume of the bubble and the volume fraction of the dispersed phase independently by adjusting the pressure applied to the gas stream, and the rate of flow of the liquid (figure 7).

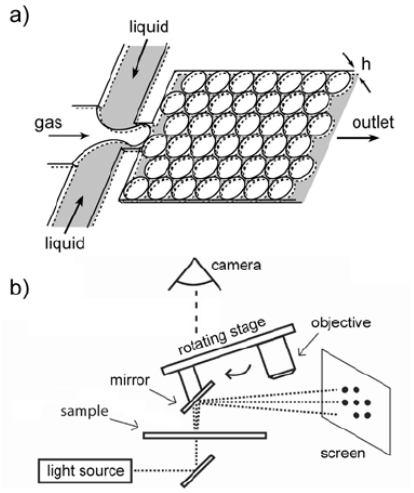

Fig.7. Schematic representations of the experimental setup. a) The flow-focusing bubble generator and self-assembled lattice of bubbles. A tank of nitrogen gas connects to the gas inlet, and digitally controlled syringes connect to the liquid inlets. The system generates monodisperse bubbles that pack into a quasi two-dimensional sheet. Cylindrical bubbles at high volume fraction pack to form a hexagonal lattice in the outlet channel: h denotes the height of the outlet channel. b) Diffraction and display of incident laser beam. Diffracted laser light orthogonal to the plane of bubble lattice is displayed on a white screen. "Sample" denotes the self-assembled flowing lattice of bubbles. We switch the objectives to observe the sample and to display the corresponding diffraction pattern.

At low volume fractions (φ_{vol}) the bubbles flowed in disordered packs (Figure 8a). As φ_{vol} increased, the packs organized into hexagonal, packed domains. At volume fractions that approached the limit of packing of disks on the plane (0.91), the domains fused into a single lattice extending throughout the outlet channel (Figures 8b-d). A further increase in the applied pressure of the gas ($\varphi_{vol} \sim 0.91$) caused the bubbles to fill the entire plane of the channel (with the liquid confined to the curved spaces between bubbles – similar to the Plateau borders) and the defects in the lattices were minimized (Figure 8c and 8d).

We used these self-assembled, tunable, lattices as diffraction gratings. These gratings can be modeled as both amplitude gratings and phase gratings. The menisci of the bubbles refract the incident light radially, in a fashion similar to diffraction gratings formed from periodic arrays of dots or holes – that is, amplitude gratings. The bubbles and the continuous medium also represent periodic arrays of alternating refractive indices – phase gratings. In a phase grating, the intensity of light at each diffraction spot is modulated by changing the phase difference of rays of interfering light that passes through the grating. In our experimental setting, the height of the channel (10 - 20 μm) and the refractive index of our continuous liquid phase (water, $n_D = 1.33$), and the wavelength of light (He-Ne laser, 632 nm) determine the phase shift of diffracted light. These parameters can be adjusted with relative ease – for example, by changing the refractive index of the continuous phase by adding salts or by changing temperature – to optimize the efficiency of the grating at a particular wavelength. In our research, we have focused on adjusting the periodicity (d) of the grating and thus changing the deflection of diffracted beams of incident radiation.

This liquid-gas grating provides several characteristics that differ from familiar solid-liquid or solid-gas gratings: i) reversible tunability in the periodicity of the grating. ii) reversible and dynamic control over the host liquid (both flow rate and composition) in real time; iii) generation and tunablility of a two-dimensional, isotropic diffraction pattern; iv) constant replacement of photobleached components.

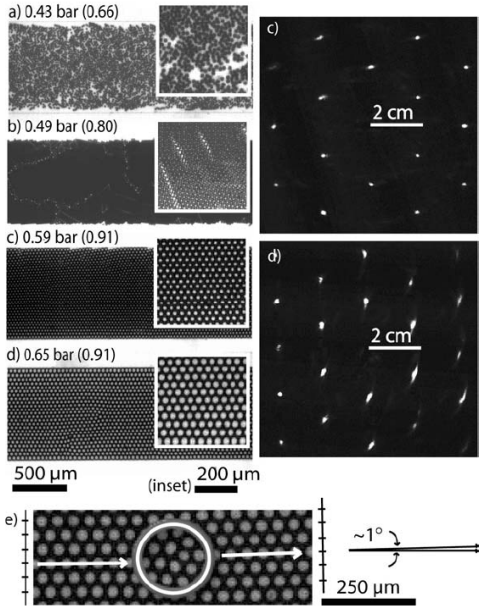

Fig.8. Packing of bubbles in a straight outlet channel that was 1-mm wide and 16-µm high. The rate of flow of the continuous phase was 0.028 µL/s. The numbers in parentheses denote the volume fraction of bubbles (φ_{vol}). a) 0.43 bar, $\varphi_{vol} = 0.66$; the volume fraction of bubble was not sufficiently high to pack the outlet channel. b) 0.49 bar, $\varphi_{vol} = 0.80$; bubbles packed as loose lattice with linear defects, and constantly reorganized the domain of packing as they flowed downstream. c) 0.59 bar, $\varphi_{vol} = 0.91$, and d) 0.65 bar, $\varphi_{vol} = 0.91$; stable packed lattices of bubbles with lattice constants of c) 34 µm and d) 51 µm (left), and their corresponding diffraction patterns (right). e) A defect in a 'stable' lattice. Even under the optimal conditions, these lattices contained occasional defects that slightly change the orientation of the lattice. The structure in the frame corresponding to 0.65 bar shows a defect – a hole – that changes the orientation of the packing. The lattice spacing remained the same, but the lattice shifted by approximated one-half of the unit cell and reoriented locally. The two white arrows show the orientation of the alignment of bubbles upstream and downstream of the hole. The orientations are off by ~1° in this example.

4. CONCLUSION

Dynamic fluidic optical components are simple to design, fabricate, and operate. They are adaptive and reconfigurable; the range of tuning is large, and only limited by the choice of liquids that can be injected into the microfluidic systems. Fluidic optical systems are also readily integrable with microanalytical and lab-on-a-chip systems for biochemical detection, where the analytes of interest are usually in the liquid or solution phase.

The development of fluidic optical systems is in its infancy. There are now enough data to establish that these systems "work" optically: one *can* guide light; one *can* make optofluidic analogs of various familiar devices; one can accomplish manipulations of light that can not be accomplished using conventional devices. The question is "Who cares?" This question cannot, yet, be answered. It is, however, possible to formulate hypotheses.

It seems unlikely that fluidic optical devices will compete with conventional, solid-state devices in optical communications (where durability, service-free operation, and stability are of paramount importance), although optofluidic systems related to those described here have been fabricated and tested for applications such as tuning the performance of in-fiber Bragg gratings. Fluidic optical systems seem, however, to be very well suited for applications in bioanalysis (where the samples are usually present in aqueous solution, and often separated using fluidic systems), and in lab-on-a-chip applications (where it is possible to use the strategy of co-fabrication to generate a range of useful functions—from analysis and generation of light to manipulation of particles using magnetic fields—in devices made using a single step of fabrication, and thus avoiding the expense and complexity of registration. A range of types of applications of aqueous solutions—in biomedicine, food testing, environmental testing, biological research, drug testing, forensics, and homeland security all seem plausible.

Fluidic optics is also opening other types of applications. For example, the ability to form wires by flowing molten solder in microfluidic channels opens the opportunity to generate moderate magnetic and electrical fields (and quite high field gradients) next to optical channels. Related systems suggest the possibility of combining optofluidics and electrochemistry. The rich and well-defined electronic states of organic and organometallic molecules—especially when coupled with very short optical path lengths—may offer opportunities for fundamentally new types of optical "materials" (fluids containing strongly absorbing materials, whose tendency to photobleach is removed as a source of concern by the dynamic character of the optofluidic systems.

Optics is an area that has followed a paradigm—solid-state fabrication focused on ultra-high optical performance and long lifetime, but with minimal adaptability. Fluidic optics suggests another paradigm: systems that only function when they operating in dissipative mode—e.g., with fluids flowing through them—and in which the systems are intrinsically unstable but highly adaptable. Time will tell the value of these characteristics.

REFERENCES

1 E. F. Borra, Astrophysical Journal **373**, 317 (1991).

2 R. Symes, R. M. Sayer, and R. J.P., PHYSICAL CHEMISTRY CHEMICAL PHYSICS **6**, 474 (2004).

3 The characteristics of fluid flow in capillaries have been studied extensively in the past. See, for example: Rosenhead, L. Laminar Boundary Layers; Dover Publications: New York, 1988. Tritton, D. J. Physical Fluid Dynamics, 2nd ed.; Oxford University Press: New York, 1988.

4 D. B. Wolfe, R. S. Conroy, P. Garstecki, B. T. Mayers, M. A. Fischbach, K. E. Paul, M. Prentiss, and G. M. Whitesides, Proceedings of the National Academy of Sciences of the United States of America **101**, 12434 (2004).

[5] R. S. Conroy, B. T. Mayers, D. V. Vezenov, D. B. Wolfe, M. G. Prentiss, and G. M. Whitesides, Applied Optics **44**, 7853 (2005).
[6] D. B. Wolfe, D. V. Vezenov, B. T. Mayers, G. M. Whitesides, R. S. Conroy, and M. G. Prentiss, Applied Physics Letters **87**, 181105/1 (2005).
[7] S. K. Y. Tang, B. T. Mayers, D. V. Vezenov, and G. M. Whitesides, Applied Physics Letters **88**, 061112/1 (2006).
[8] B. T. Mayers, D. V. Vezenov, V. I. Vullev, and G. M. Whitesides, Analytical Chemistry **77**, 1310 (2005).
[9] D. V. Vezenov, B. T. Mayers, R. S. Conroy, G. M. Whitesides, P. T. Snee, Y. Chan, D. G. Nocera, and M. G. Bawendi, Journal of the American Chemical Society **127**, 8952 (2005).
[10] D. V. Vezenov, B. T. Mayers, D. B. Wolfe, and G. M. Whitesides, Applied Physics Letters **86**, 041104/1 (2005).
[11] M. Hashimoto, B. T. Mayers, P. Garstecki, and G. M. Whitesides, Small **In press** (2006).
[12] T. Deng, H. Wu, S. T. Brittain, and G. M. Whitesides, Analytical Chemistry **72**, 3176 (2000).
[13] R. J. Jackman and G. M. Whitesides, Chemtech **29**, 18 (1999).
[14] R. S. Kane, S. Takayama, E. Ostuni, D. E. Ingber, and G. M. Whitesides, Biomaterials **20**, 2363 (1999).
[15] J. C. McDonald, D. C. Duffy, J. R. Anderson, D. T. Chiu, H. Wu, O. J. Schueller, and G. M. Whitesides, Electrophoresis **21**, 27 (2000).
[16] M. K. Ng Jessamine, I. Gitlin, D. Stroock Abraham, and M. Whitesides George, Electrophoresis **23**, 3461 (2002).
[17] T. W. Odom, J. C. Love, D. B. Wolfe, K. E. Paul, and G. M. Whitesides, Langmuir **18**, 5314 (2002).
[18] K. E. Paul, M. Prentiss, and G. M. Whitesides, Advanced Functional Materials **13**, 259 (2003).
[19] G. M. Whitesides, E. Ostuni, S. Takayama, X. Jiang, and D. E. Ingber, Annual Review of Biomedical Engineering **3**, 335 (2001).
[20] G. M. Whitesides, E. Ostuni, S. Takayama, X. Jiang, and D. E. Ingber, Annual review of biomedical engineering **3**, 335 (2001).
[21] Y. Xia and G. M. Whitesides, Polymeric Materials Science and Engineering **77**, 596 (1997).
[22] Y. Xia and G. M. Whitesides, Annual Review of Materials Science **28**, 153 (1998).
[23] Y. Xia and G. M. Whitesides, Angewandte Chemie, International Edition **37**, 550 (1998).
[24] B. D. Gates and G. M. Whitesides, Journal of the American Chemical Society **125**, 14986 (2003).
[25] Unpublished.
[26] K. Hoshino and I. Shimoyama, JOURNAL OF MICROMECHANICS AND MICROENGINEERING **13**, 149 (2003).
[27] J. N. Lee, C. Park, and G. M. Whitesides, Analytical Chemistry **75**, 6544 (2003).
[28] P. Garstecki, I. Gitlin, W. DiLuzio, G. M. Whitesides, E. Kumacheva, and H. A. Stone, Applied Physics Letters **85**, 2649 (2004).
[29] P. Garstecki, A. M. Ganan-Calvo, and G. M. Whitesides, Bulletin of the Polish Academy of Sciences: Technical Sciences **53**, 361 (2005).
[30] P. Garstecki, M. J. Fuerstman, and G. M. Whitesides, Nature Physics **1**, 168 (2005).
[31] P. Garstecki, M. A. Fischbach, and G. M. Whitesides, Applied Physics Letters **86**, 244108/1 (2005).

[32] P. Garstecki, M. J. Fuerstman, and G. M. Whitesides, Physical Review Letters **94**, 234502/1 (2005).
[33] P. Garstecki, J. Fuerstman Michael, and M. Whitesides George, Physical review letters **94**, 234502. (2005).
[34] P. Garstecki and G. M. Whitesides, Physical Review Letters **97**, 024503/1 (2006).
[35] P. Garstecki, M. J. Fuerstman, H. A. Stone, and G. M. Whitesides, Lab on a Chip **6**, 437 (2006).
[36] P. Garstecki, M. J. Fuerstman, M. A. Fischbach, S. K. Sia, and G. M. Whitesides, Lab on a Chip **6**, 207 (2006).
[37] P. Garstecki and M. Whitesides George, Physical review letters **97**, 024503 (2006).
[38] P. Garstecki, J. Fuerstman Michael, A. Stone Howard, and M. Whitesides George, Lab on a chip **6**, 437 (2006).
[39] P. Garstecki, J. F. Michael, A. Fischbach Michael, K. Sia Samuel, and M. Whitesides George, Lab on a chip **6**, 207 (2006).